Insights into the Summer Diurnal Cycle over Eastern South Africa

SHUNYA KOSEKI

Geophysical Institute, University of Bergen, and Bjerknes Centre for Climate Research, Bergen, Norway

BENJAMIN POHL

Centre de Recherches de Climatologie, UMR6282, Biogéosciences, CNRS, and Université de Bourgogne Franche-Comté, Dijon, France

BHUWAN CHANDRA BHATT

Geophysical Institute, University of Bergen, and Bjerknes Centre for Climate Research, Bergen, Norway

NOEL KEENLYSIDE

Geophysical Institute, University of Bergen, and Nansen Environmental and Remote Sensing Center, and Bjerknes Centre for Climate Research, Bergen, Norway

ARIELLE STELA NKWINKWA NJOUODO

Department of Oceanography, MARE Institute, and Nansen-Tutu Centre for Marine Environmental Research, University of Cape Town, Cape Town, South Africa

(Manuscript received 27 May 2018, in final form 11 October 2018)

ABSTRACT

Adopting a state-of-the-art numerical model system, we investigate how the diurnal variations in precipitation and local breeze systems are characterized by lower-boundary conditions related to the Drakensberg highland and warm SST associated with the Agulhas Current. A control simulation can simulate the hydrometeorological climates in the region realistically, but the terrestrial rainfall is overestimated. During daytime, the precipitation is confined to the Drakensberg highland, and there is an onshore local breeze, while during midnight to morning, the rainfall is confined to the Agulhas Current, and the breeze is offshore. These variations are captured by the numerical simulation, although the timing of maximum rainfall is early over the land and delayed over the ocean. The sensitivity experiment in which the Drakensberg is absent shows a drastic modification in the diurnal variations over land and ocean. The terrestrial precipitation is largely decreased around the Drakensberg and is largest along the coast during daytime. The nocturnal marine precipitation along the Agulhas Current is also reduced. Although the daily residual breeze is still pronounced even without the Drakensberg, wind speed is weakened. We attribute this to the reduction of precipitation. In another sensitivity experiment with smoothened warm SST due to the Agulhas Current, the amplitudes of diurnal variations are not modified remarkably, but the coastal rainfall is diminished to some extent due to less evaporation along the Agulhas Current. This study concludes that the Drakensberg plays a crucial role for the diurnal cycle, and the impact of the Agulhas Current is limited on the diurnal cycle of the coastal precipitation in this region.

1. Introduction

South African precipitation variability shapes the regional and local economies, as most of the southern African nations rely largely on the rain-fed agriculture. A clear contrast between dry winter (June–August) and wet summer (November–March; NDJFM) conditions over the southern African region represents a large annual cycle characteristic of the southern African

Supplemental information related to this paper is available at the Journals Online website: https://doi.org/10.1175/MWR-D-18-0184.s1.

Corresponding author: Shunya Koseki, shunya.koseki@gfi.uib.no

DOI: 10.1175/MWR-D-18-0184.1

precipitation (e.g., Pohl et al. 2007; MacKella et al. 2014; Lawal et al. 2015; Gergis and Henley 2017). The summer season precipitation is of great importance. In addition to the precipitation, the associated terrestrial hydrological processes need to be taken into account for the mitigation and prevention of natural disasters such as drought and flooding (e.g., Li et al. 2015). As southern Africa is in the subtropics, the amplitude of daily variation in incoming solar radiation is strong, and there is a pronounced diurnal variation in cumulus convection. Recently, a first look at the diurnal cycle over the entirety of South Africa was performed by Rouault et al. (2013), and a state-of-the-art regional climate modeling was used by Pohl et al. (2014). The knowledge of the precipitation diurnal cycle has practical importance in understanding the energy budget and water balance and in applications of water resource management, hydrology, and air quality modeling.

In the tropics, cumulus convection and associated precipitation are characterized by a diurnal cycle, which has been discussed in many previous studies. Yang and Smith (2006) examined the diurnal cycle over the global tropics and suggested that heavy precipitation areas exhibit strong diurnal variations. There are also notable regional studies on the diurnal cycle (e.g., in the western Pacific warm pool; Chen and Houze 1997) in the Maritime Continent (e.g., Teo et al. 2011; Koseki et al. 2013; Bhatt et al. 2016). The diurnal cycle over land is driven by a thermal contrast between terrestrial and marine surfaces, caused, in a first order, by incoming solar radiation flux and differences in the heat contents. Onshore sea breeze in daytime to evening (offshore land breeze in midnight to morning) initiates low-level convergence and cumulus convection over land (sea) (Estoque 1962). Besides the land/sea breezes, diurnal variation related to the mountain- and valley-breeze systems are generated by the differences in heating due to complex terrain structures (e.g., Nesbitt and Zipser 2003) over the landmass. This system also shows a clear diurnal variation and enhances cumulus convection over the land. These above circulation systems are influenced by larger-scale background wind as well (e.g., Koseki et al. 2013).

While the diurnal cycle in the tropics has received much attention, there are relatively few studies on the diurnal cycle in the subtropics. This may be because cumulus convection is weaker, compared to that in the tropics, and subsidence associated with the subtropical high is dominant and tends to inhibit cumulus convection. Certain regions in the subtropics, such as South Africa, also exhibit a diurnal cycle. Rouault et al. (2013) found a clear diurnal variation of precipitation over South Africa in the austral summer (November–March) using hourly rain gauge records. Terrestrial precipitation is dominant in afternoon to evening, while coastal regions over the sea exhibit midnight-to-morning precipitation over the Agulhas Current. Because the Agulhas Current transports the tropical warm water from the tropics toward the subtropics and extratropics (e.g., Webb 1999; Boebel et al. 2003; Backeberg et al. 2009), cumulus convection and cloud formation are enhanced by the warm Agulhas Current along the eastern coast of South Africa (e.g., Lutjeharms et al. 1986; Jury et al. 1993; Nkwinkwa Njouodo et al. 2018).

The dynamical mechanism for the diurnal cycle in this region is not well understood quantitatively and may be influenced by the orography and ocean currents. We revisit the diurnal cycle and provide insights into the dynamical aspects, which have not been elucidated yet. In addition to the role of SST, the complex topography of the Drakensberg highland (topographic height up to 3482 m), which sits along the eastern coast of South Africa, may also have a role in modulating the diurnal cycle. The mountain–valley circulation in the Drakensberg could modify the deep atmospheric convection (e.g., Joseph et al. 2008). It is known that the high elevated orography over southern Africa (including the Drakensberg) influences the atmospheric circulation over the South Atlantic (e.g., Richter and Mechoso 2004; Potter et al. 2017). While the contributions of the abovementioned terrain and SST to the diurnal cycle of precipitation have been witnessed with in situ observations (e.g., Preston-Whyte 1970a,b; Tyson and Preston-Whyte 1972), there are few studies with a state-of-the-art numerical model, and a quantitative assessment has not been given yet. This paper extends on previous studies by Tyson and Preston-Whyte (1972), Rouault et al. (2013), and Pohl et al. (2014). The aim of this paper is to provide a more complete dynamical understanding of the diurnal cycle of precipitation in this region. We hypothesize that the characteristic lower-boundary conditions, such the complex Drakensberg highland and sharp gradient of warm SST due to the Agulhas Current, modulate the diurnal variations in precipitation and in local circulation systems over eastern South Africa.

Thus, the present study investigates the diurnal cycle of precipitation in the austral summer season (November–March) over eastern South Africa and associated atmospheric dynamics by conducting sensitivity experiments using a high-resolution state-of-the-art regional climate model. This paper is structured as follows. Section 2 provides the data and model utilized and methodology for the analysis. We revisit the diurnal cycle over the region and evaluate the model performance in section 3. The results of sensitivity experiments are given in section 4. Discussion and summary are provided in section 5.

2. Data and model

a. Observation and reanalysis

The 3-hourly and 0.25° × 0.25° grid resolution Tropical Rainfall Measuring Mission (TRMM-3B42; Huffman et al. 2007) is used for evaluation of the modeled precipitation. The 3-hourly temporal resolution provides eight data points over 1 day, which is sufficient to enable diagnosis of diurnal variability, and the 25-km resolution resolves meso-alpha-scale diurnal features. The 6-hourly and 0.75° × 0.75° grid resolution ERA-Interim (Dee et al. 2011) datasets are employed both for characterizing the climatological state and as lateral boundary conditions for the numerical experiments. In addition, the data from the Famine Early Warning Systems Network (FEWS NET) Land Data Assimilation System (FLDAS; at 0.1° × 0.1° grid resolution) are also used. This system is based on the Noah land surface model (Chen and Dudhia 2001a,b), which is forced by observed and reanalyzed meteorological boundary conditions. More details can be seen in McNally et al. (2017). Here, we use data from the five summer seasons (November–March) from 2001 to 2005. There is considerable consistency between the characteristics of the summer season diurnal cycle from year to year (not shown), and this suggests that 5 years of summer season data are sufficient to characterize the climatology.

b. Weather Research and Forecasting Model

1) Configuration of WRF

The Advanced Research version of the Weather Research and Forecasting (WRF) Model (WRF-ARW, hereafter WRF; Skamarock et al. 2008), version 3.7.1, is employed to investigate the diurnal cycle of precipitation and associated dynamics over eastern South Africa. The model domain (Fig. 1) covers the region of 43°–17°S and 8°–52°E. The spatial resolution is 25 km (172 × 117 grid cells) with 56 vertical eta-coordinate levels (one terrain-following vertical coordinate; see http://glossary.ametsoc.org/wiki/Eta_vertical_coordinate) with 22 levels below $\eta = 0.85$ to represent the lower atmosphere in more detail. The WRF Model is forced laterally by 6-hourly ERA-Interim and at the surface by the daily Optimum Interpolation Sea Surface Temperature (OISST; at 0.25° × 0.25° grid resolution; Reynolds et al. 2007). A relaxation zone is implemented in the first four lateral grid points to avoid discontinuity between forcing data and the model. The simulation extends from 1 December 2000 to 1 January 2006. The first month is considered as spinup, and only the remaining 5 years are analyzed.

The following physical schemes used in WRF are the WRF single-moment 6-class microphysics scheme (WSM6; Hong and Lim 2006) and the Yonsei University parameterization for the planetary boundary layer (PBL; Hong et al. 2006). The longwave and shortwave radiative forcings are parameterized by the Rapid Radiative Transfer Model (Mlawer et al. 1997) schemes. We selected these schemes as they were used by Pohl et al. (2014) to successfully simulate the diurnal cycle of South African rainfall. Over land, the Noah land surface model consisted of four layers of soil (Chen and Dudhia 2001a,b). For cumulus convective parameterization, we use the Kain–Fritsch (KF; Kain 2004) scheme since we found it to better represent the horizontal pattern of precipitation associated with the Agulhas Current than the other available convection schemes (not shown).

2) Sensitivity experiments

One control and two sensitivity experiments are performed in this study. The control experiment (referred to as WRF-CTL) has the settings in section 2b(1). A first sensitivity experiment is performed in which topography of the Drakensberg is set to zero altitude, and land use is identical to WRF-CTL (referred to as WRF-NODB). A second sensitivity experiment is with smoothened SST boundary conditions (referred to as WRF-SMTH). The configuration of both sensitivity experiments is otherwise identical to WRF-CTL. The SST is smoothened by a spatial filter based on a nine-neighbor grid method that is applied 100 times only around the Agulhas Current. This method weakens the sharp SST gradients associated with the warm SST with the Agulhas Current, but does not reduce the SST associated with the Agulhas Current completely. The modified boundary conditions for these sensitivity experiments are shown in Fig. 1. Additional sensitivity experiments were performed to investigate the sensitivity of the results to choices of model and its physical parameterization (see the details of experiments in section 4d).

3. Evaluation of WRF simulations

a. NDJFM-mean state

In this subsection, we evaluate the performance of the WRF-CTL simulation in representing monthly mean of precipitation and wind fields by comparing it to observations and reanalysis data. During the summer season, most of the terrestrial precipitation is concentrated on the eastern side of South Africa, and the western part of South Africa is arid (Fig. 2a). The marine precipitation is largest over the Agulhas Current (e.g., Jury et al. 1993; Nkwinkwa Njouodo et al. 2018) and extends to the south

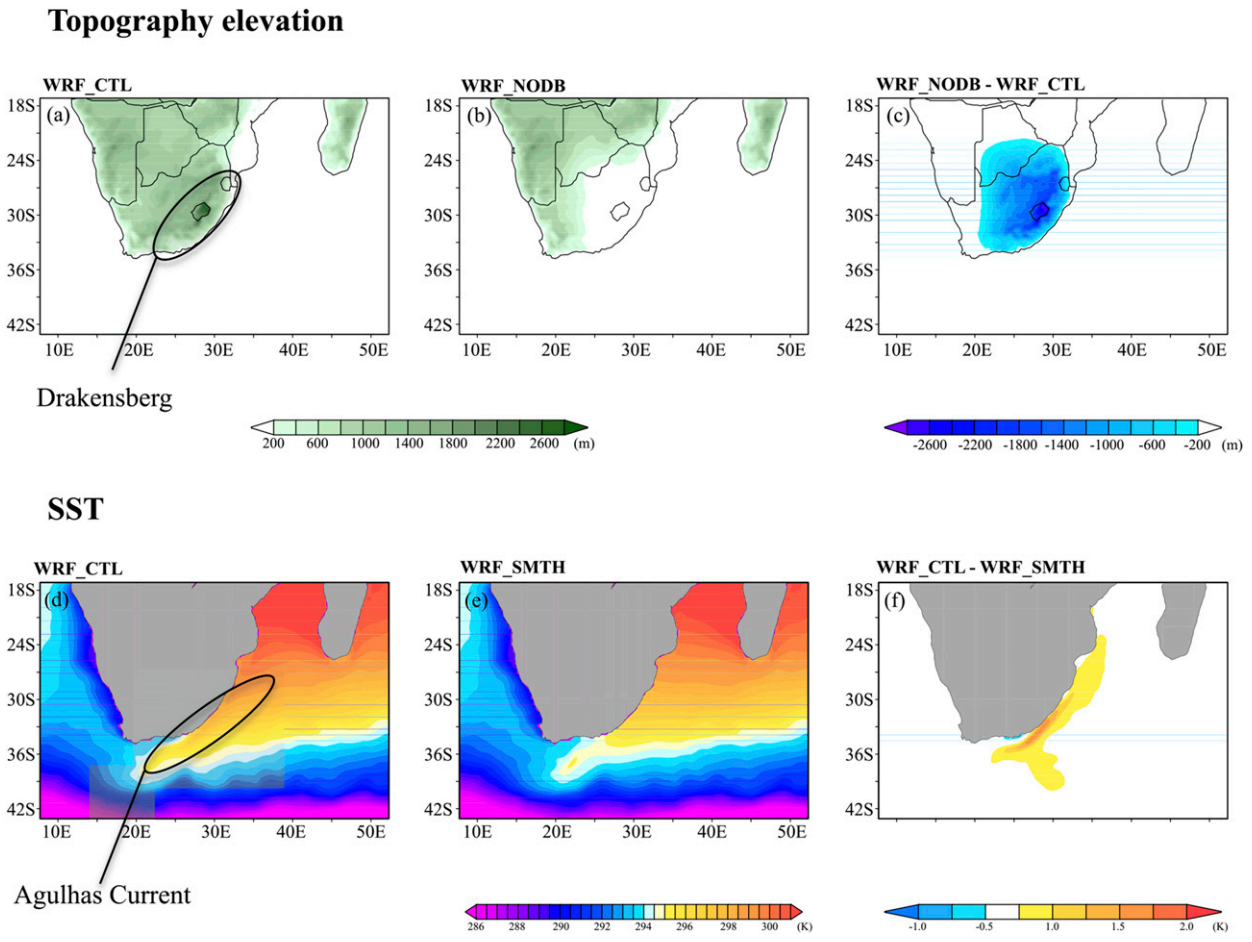

FIG. 1. (a) Simulation domain with topography, as used in WRF-CTL simulations. (b) As in (a), but for WRF-NODB (with no Drakensberg). (c) Difference between (b) and (a). (d) Mean SST horizontal distribution in WRF-CTL simulations. (e) As in (d), but for WRF-SMTH (with smoothed Agulhas Current). (f) Difference between (e) and (d). Refer to text for more explanations on the WRF sensitivity experiments.

Indian convergence zone (SICZ; e.g., Cook 2000). The terrestrial precipitation is overestimated in particular around the Drakensberg, but its distribution is in good qualitative agreement with the observations (Fig. 2d). The marine precipitation is quantitatively well reproduced by the model. The easterly surface wind to the east of South Africa is linked to the Mascarene subtropical high pressure system over the southern Indian Ocean (Fig. 2a).

The wind pattern is also realistically modeled, but the easterly component is overly strong (Fig. 2d). The observations show that the land surface hydrological variables are closely associated with the terrestrial precipitation (Figs. 2b,c): the soil moisture at the first layer and evaporation from the land surface are at maximum around the Drakensberg. While the WRF-CTL simulates the pattern of the terrestrial hydrological quantities qualitatively well, the land surface is too wet (Fig. 2e), and the evaporation is too strong (Fig. 2f), compared to the reanalysis. Cosgrove et al. (2003) and Chen et al. (2007) suggested that a long-term spinup of 3–10 months is desirable for the land surface processes in the land data assimilation system. Two different climatologies of soil moisture at the first layer (one is the same as Fig. 2e, and the other is climatology excluding January–March 2001, meaning 1-yr spinup) are estimated, and they are found to be nearly identical (not shown). This indicates that the short spinup does not affect the soil moisture climatology in our case. Moreover, these evaluations are performed using the statistical methods (summarized statistically in Table 1). As one of them, we use the root-mean-square error (RMSE). Although the terrestrial precipitation is very biased ($2.712\,\mathrm{mm\,day^{-1}}$), the geographical pattern is better represented (pattern correlation is 0.78) than the marine precipitation (0.68 pattern correlation). The 10-m horizontal wind is well represented in terms of its distribution (pattern

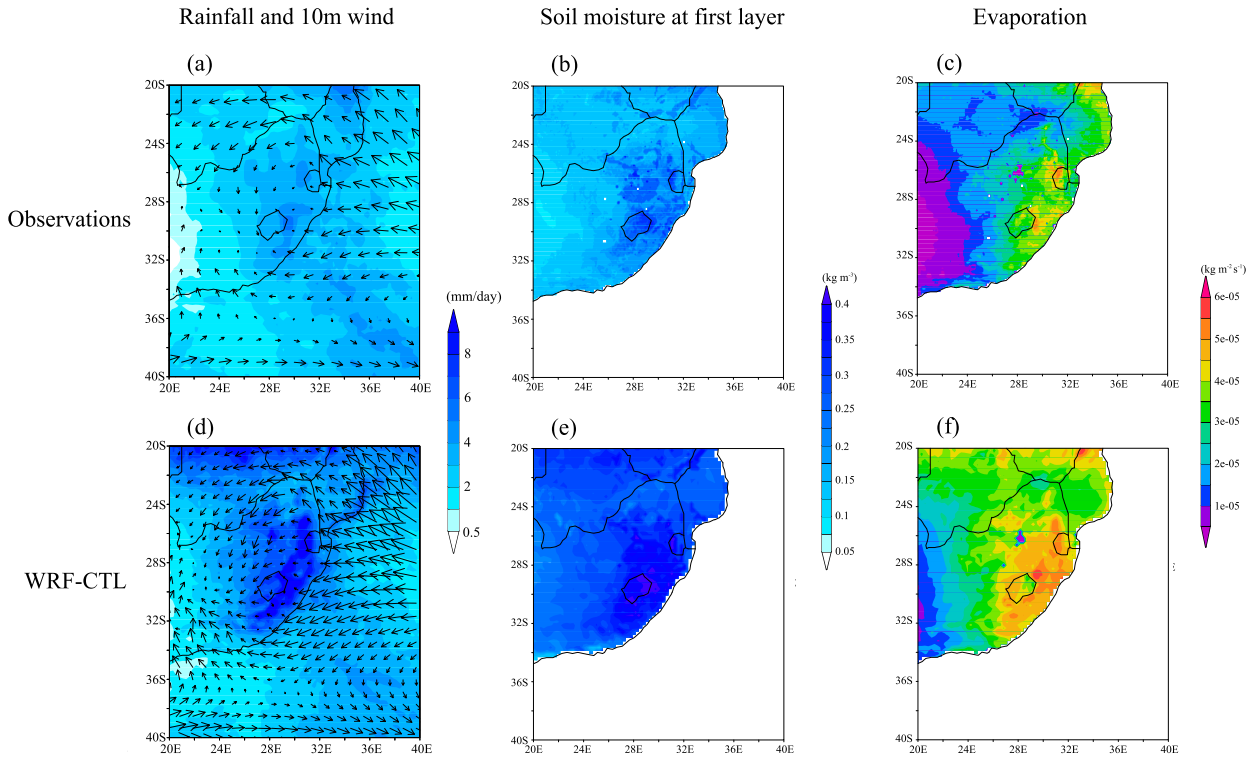

FIG. 2. Austral summer season (NDJFM, 2001–05) mean climatology (top) from the TRMM-3B42 and FLDAS (a) precipitation and 10-m wind, (b) soil moisture at the first layer, and (c) evaporation, and (bottom) from the WRF-CTL (d) precipitation and 10-m wind, (e) soil moisture at the first layer, and (f) evaporation.

correlations are 0.94 and 0.95 for zonal and meridional winds, respectively). The domain for these statistical calculations is 40°–20°S and 20°–40°E and excludes the one grid for forcing and four grids for relaxation with the lateral boundary conditions. However, note that the inner domain of the model is still influenced by the lateral boundary condition (Crétat et al. 2011), and the statistics—in particular, 10-m wind—might include the effects of the lateral boundary condition. On the other hand, the precipitation can be less dependent on the lateral boundary condition since its behavior is determined strongly by the cumulus scheme.

TABLE 1. Statistical values of RMSE and pattern correlation for WRF-CTL evaluation. The domain covers 40°–20°S and 20°–40°E.

	RMSE	Pattern correlation
Terrestrial precipitation	2.712 (mm day^{-1})	0.7790
Marine precipitation	0.5394 (mm day^{-1})	0.6834
Soil moisture	0.086 (m^3 m^3)	0.8397
Evaporation	1.357×10^{-5} (kg m^{-2} s^{-1})	0.8646
10-m zonal wind	0.7374 (m s^{-1})	0.9432
10-m meridional wind	0.5521 (m s^{-1})	0.9475

b. *Observed and modeled diurnal cycle*

The diurnal variation of precipitation in this region has been overviewed by Rouault et al. (2013) and Pohl et al. (2014). Here, we revisit the diurnal cycle in precipitation, paying more attention to the local circulation.

Figure 3 gives 3-hourly observed precipitation from TRMM-3B42 and 6-hourly daily residual component of 10-m winds of ERA-Interim at local standard time (LST). The LST (UTC + 2 h) is used in our analysis hereafter. The daily residual component is calculated by

$$u'(t) = u(t) - \overline{u} \quad \text{and} \quad v'(t) = v(t) - \overline{v}, \tag{1}$$

where the overbar and prime denote daily mean and daily residual components of 10-m winds, and t is the time step of the data. To keep the raw information of ERA-Interim, no interpolation is employed for 6-hourly winds to have 3-hourly winds.

Between 0200–0500 and 1100–1400 LST (midnight to early afternoon), a main cluster of precipitation is dominant over the ocean along the Agulhas Current, and the daily residual wind is offshore and downhill. The daily residual wind is divergent around the Drakensberg. This daily residual surface wind pattern is indicative of a

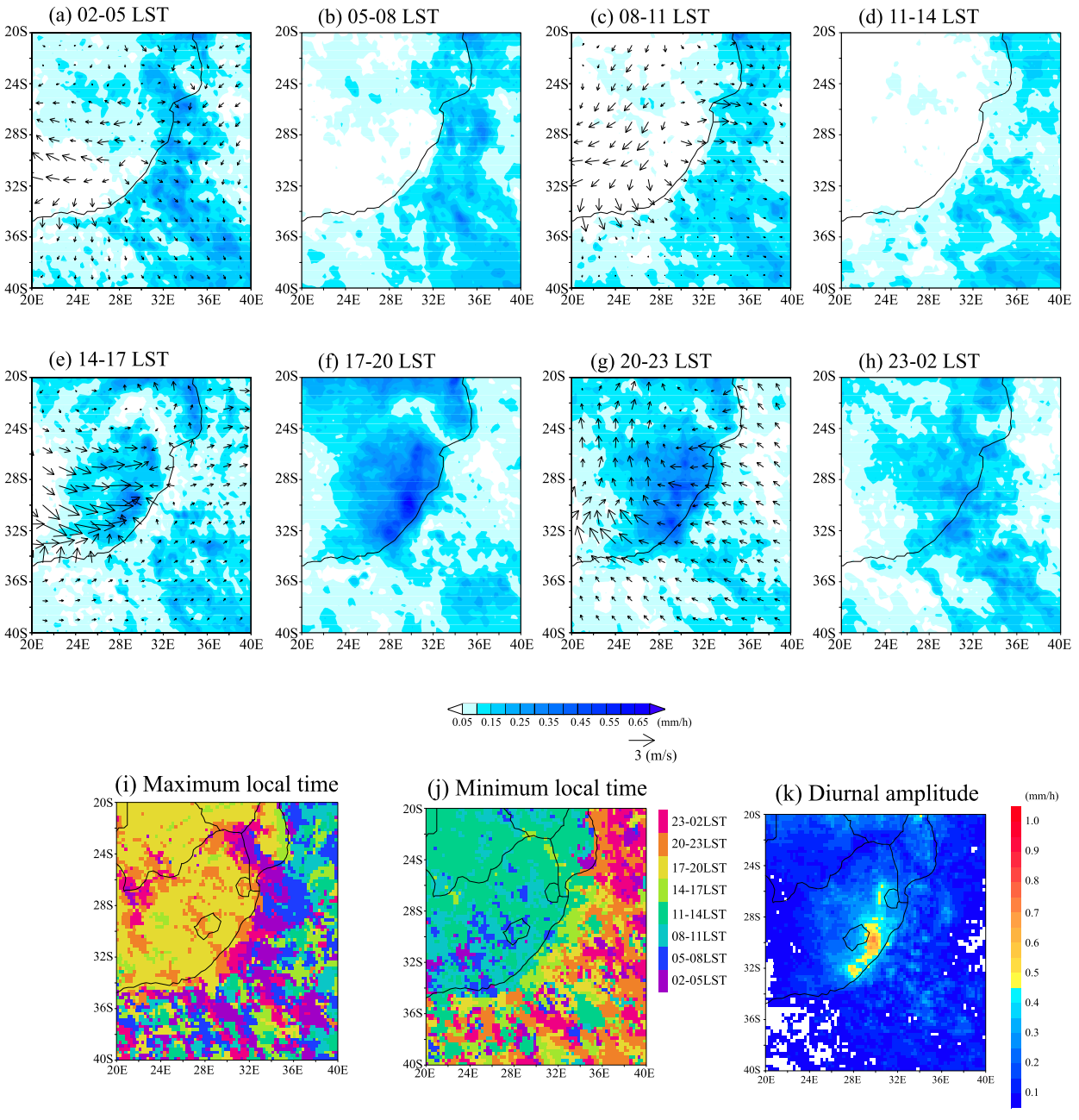

FIG. 3. (a)–(h) Austral summer season (NDJFM, 2001–05) mean climatology of 3-hourly precipitation from TRMM 3B42 (color) and the 6-hourly diurnal residual components of 10-m wind from daily means of ERA-Interim (vectors). (i) and (j) Local time for maximum and minimum rainfall during the summer season at each grid. (k) Rainfall amplitude between maximum and minimum.

land-/mountain-breeze circulation that generates convergence (not shown) and associated precipitation over the ocean. On the other hand, at 1400–1700 LST, terrestrial precipitation becomes enhanced around the Drakensberg and nearby coastal regions, and there is onshore daily residual surface wind (suggesting the sea-/valley-breeze circulation). Consequently, there is strong daily residual surface wind convergence over the terrain. Between 1700–2000 and 2000–2300 LST, precipitation is still vigorous over the land, and marine precipitation strengthens close to the eastern coast. In particular, at 2000–2300 LST, there is a certain change in the local daily residual circulation: while the onshore land breeze still exists (although it is weakened, compared to that at 1400–1700 LST), the uphill winds almost disappear. At 2300–0200 LST, the cluster of precipitation moves more

offshore. The period from 2000–2300 to 2300–0200 LST is a regime transition from the terrestrial to marine precipitation. These sea-/land-breeze circulations are consistent with the well-established nature of the local winds observed by Tyson and Preston-Whyte (1972).

Figures 3i–k present the local standard time of maximum and minimum precipitation at each grid point and the amplitude of precipitation (defined as the difference between precipitation at maximum and minimum) for the observation. Over most of the land, the observed maximum time is 1700–2000 LST. Over the coastal sea, the observed maximum time is approximately between 2300–0200 and 0200–0500 LST (Fig. 3i), and the observed minimum time is early to late morning (0500–0800 to 0800–1100 LST; Fig. 3j) over the land. As shown in Fig. 3k, the diurnal amplitude of precipitation is quite large around the Drakensberg and is moderate over the Agulhas Current in the observations. Both maximum and minimum times over the open Indian Ocean look patchy. This can be because the open ocean is far from the landmass of the African continent, and the marine precipitation is not generated mainly by the diurnal cycle over the open ocean where the diurnal amplitude is small.

Basically, the WRF-CTL is able to simulate the diurnal variation in the precipitation and local daily residual flow, as shown in Figs. 4a–h. However, the WRF-CTL overestimates terrestrial precipitation (Fig. 2). The divergence is created by local residual flows; nevertheless, some rainfall is still simulated over the land even during night and morning times (0200–0500 to 0800–1100 LST). Terrestrial precipitation at 1100–1400 LST is vigorous in WRF-CTL, but there is little observed terrestrial precipitation at this time of day (see Fig. 3d), and the simulated peak time of terrestrial precipitation is at 1400–1700 LST, which is earlier than the observations. The poor combination of physical schemes might cause such errors (e.g., Pohl et al. 2014). In this study, the Kain–Fritsch scheme is selected because it better represents the narrow precipitation band associated with the Agulhas Current, as compared to the Betts–Miller–Janjić (Janjić 1994) and Grell–Freitas (Grell and Freitas 2014) schemes available in WRF (not shown). Additionally, this is a common issue of early triggering in the WRF simulation and other regional climate modeling (e.g., Nikulin et al. 2012; Pohl et al. 2014; Bhatt et al. 2016). However, the transition of regime from sea breeze to land breeze is well reproduced (Figs. 4g,h). More details of the local sea-/land-breeze system will be given in section 4b. As Figs. 4i–k show, while the simulated maximum and minimum times are mostly 3 h earlier than the observation, and the diurnal amplitude of precipitation is too strong around the Drakensberg, their horizontal distributions are better captured, particularly over the land. Contrastingly, the amplitude over the Agulhas Current is well simulated in WRF-CTL.

As the Drakensberg is a complex terrain with steep gradient, the daily residual circulation can be influenced by the topography gradient as mountain–valley breeze circulation (in the WRF grid, the maximum gradient is about $0.025\,\mathrm{m\,m^{-1}}$ around the top of the Drakensberg). Here, we assess the topography–circulation interaction. To associate the daily residual winds with the topography gradient, a dot production P between the topography gradient vector $\mathbf{G}$ and the daily residual wind vector $\mathbf{U}$ is estimated as

$$P(t) = \mathbf{G} \cdot \mathbf{U} = (Z_x, Z_y) \cdot [u'(t), v'(t)] = |\mathbf{G}||\mathbf{U}| \cos\alpha . \quad (2)$$

Here, Z is the topography height, and its subscripts denote horizontal differentiation. Parameter α is an angle between vectors $\mathbf{G}$ and $\mathbf{U}$. During the morning (0200–0500 to 0500–0800 LST), the dot production is highly negative around the Drakensberg in WRF-CTL (Fig. 5). This negative value indicates that the daily residual winds blow in the opposite direction ($\pi/2 < \alpha \le \pi$) of the topography gradient. That is, the circulation is associated with downhill mountain breeze. At 0800–1100 LST, there is a mixture of negative and positive values, indicating the transition phase from onshore to offshore winds. On the other hand, during the afternoon to evening (1100–1400 to 1400–1700 LST), the dot production turns positive, suggesting that the local daily residual winds flow in the same direction ($0 \le \alpha < \pi/2$) as the topography gradient. These winds are uphill and represent a valley-breeze circulation that enhances cumulus convection over the topographic region. At 1700–2000 LST, two phases of onshore and offshore winds appear again. From 2000–2300 to 2300–0200 LST, there is a reversal of the sign from the positive to the negative dot product, indicating the transition of valley- to mountain-breeze circulation. Tyson (1968a,b) indicated that the Drakensberg drives the daytime uphill and nocturnal downhill local winds, and our simulation shows consistent results.

4. Results of sensitivity experiments

In the previous section, we revisited the summer diurnal cycle of precipitation over eastern South Africa and showed that the WRF-CTL simulates the diurnal variation in the precipitation and local daily residual circulation. In this section, we compare the results of sensitivity experiments of WRF-NODB and WRF-SMTH (see section 2) with the WRF-CTL to explore how the diurnal cycle of precipitation and local daily residual circulation is

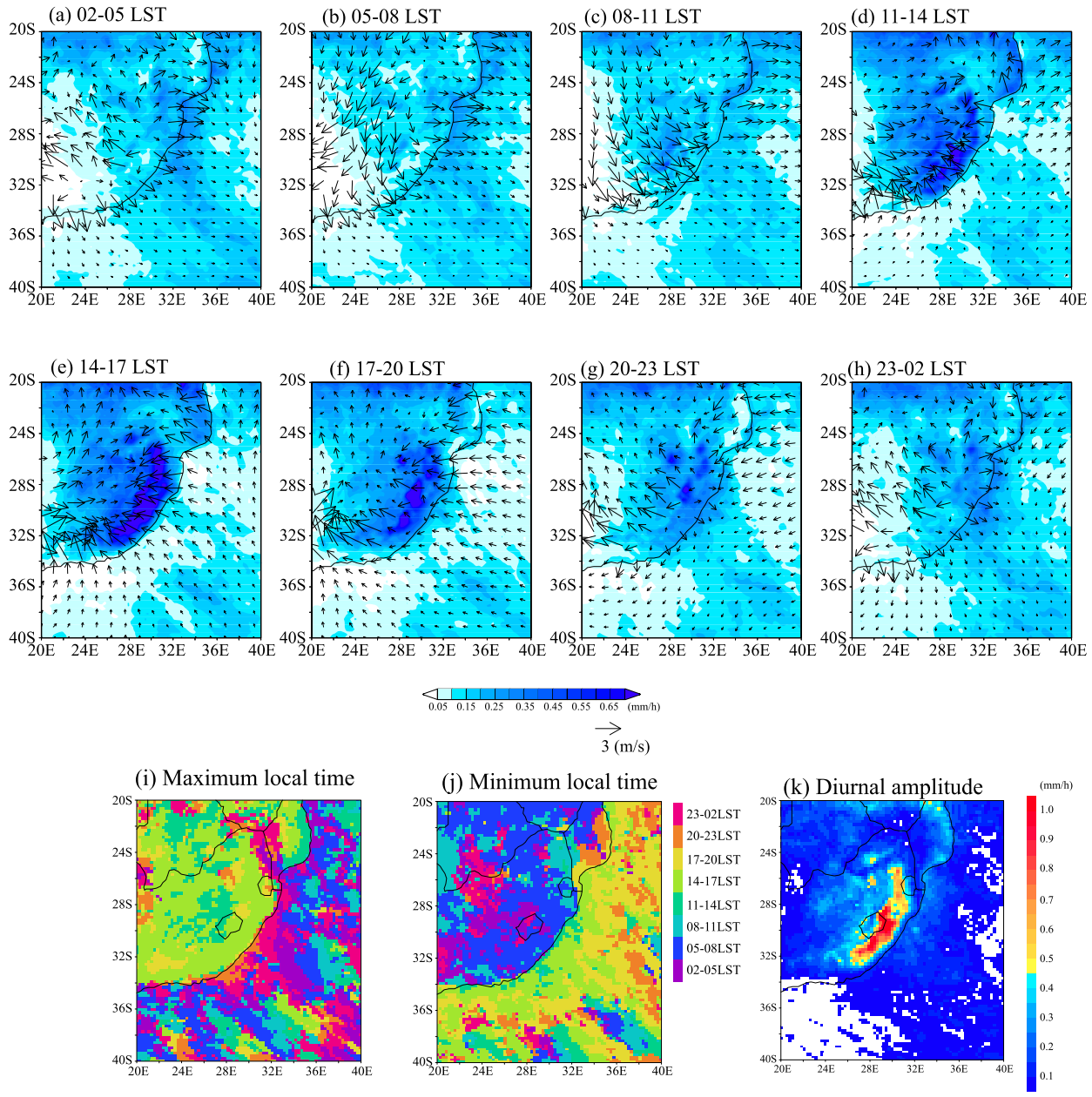

FIG. 4. As in Fig. 3, but for WRF-CTL simulation with the 3-hourly residuals from daily mean10-m wind.

modulated by the Drakensberg and SST gradients associated with the Agulhas Current, respectively.

a. NDJFM-mean state in the sensitivity experiments

Before analyzing the diurnal cycle, we investigate the impact of changed boundary condition on NDJFM-mean precipitation (Fig. 6). Eliminating the Drakensberg from the terrain boundary condition (WRF-NODB) drastically suppresses the terrestrial precipitation around the mountains (Figs. 6a,b). This indicates that the terrestrial precipitation over highland South Africa is triggered significantly by the Drakensberg (approximately 75% due to cumulus convection and 25% due to large-scale condensation; not shown). Interestingly, WRF-NODM simulates a large decrease in marine precipitation over the ocean from the Agulhas Current to the SICZ (36°–32°S, 32°–38°E). An anomalous anticlockwise circulation is generated around South Africa in WRF-NODB, and there are anomalous high sea level pressure and high geopotential heights over the SICZ (not shown). These

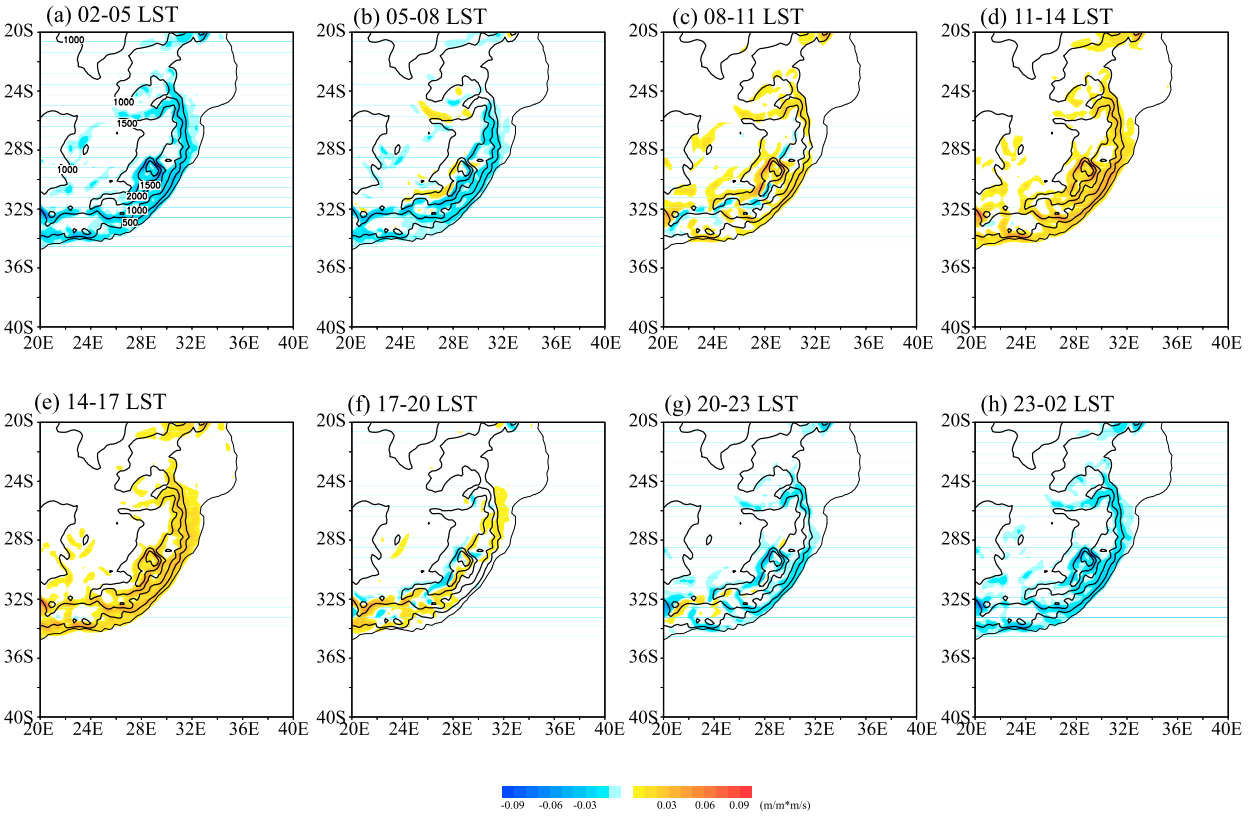

FIG. 5. As in Figs. 4a–h, but for the dot product of topography gradient vector and daily residual 10-m wind in WRF-CTL.

high pressure anomalies will act to suppress the convection over the SICZ. On the other hand, the terrestrial precipitation west of the Drakensberg (southwestern South Africa) is enhanced in the WRF-NODB. This interesting feature is demonstrated in our other research (Koseki and Demissie 2018). Previous studies have shown that the southern African topographies, including the Drakensberg, have an important impact on the large-scale atmospheric circulation and marine stratocumulus formation over the southern Atlantic (e.g., Richter and Mechoso 2004; Potter et al. 2017).

Smoothing the SST associated with the Agulhas Current (WRF-SMTH) reduces marine precipitation along the Agulhas Current (Figs. 6c,d), compared to WRF-CTL, although its significance is limited along the coast. According to Nkwinkwa Njouodo et al. (2018), the warm SST due to the Agulhas Current enhances the low-level convergence and, consequently, the precipitation. While they focus on the annual mean, the marine precipitation in summer is also reduced by as much as 40% along the Agulhas Current in the WRF-SMTH. The terrestrial precipitation is also weakened over the coastal region, but significance is weak.

Table 2 summarizes the statistics of precipitation difference between WRF-CTL and the sensitivity experiments. The horizontal distribution of the precipitation is highly modulated over the land and ocean in WRF-NODB, compared to WRF-CTL: the terrestrial precipitation loses most of the realistic horizontal distribution in the absence of the Drakensberg, and the pattern correlation between the runs is only 0.23. The distribution of marine precipitation is also modestly affected, with the pattern correlation of 0.63 between the runs. On the other hand, in WRF-SMTH, both terrestrial and marine precipitations maintain similar horizontal distributions to those in WRF-CTL (with pattern correlations of more than 0.90).

b. Diurnal cycle in the WRF-NODB

The NDJFM-mean precipitation (Fig. 6a) is divided into 3-hourly precipitation with the local daily residual 10-m winds (Fig. 7). A diurnal variation in precipitation is still generated in the WRF-NODB, but it differs remarkably from that in the WRF-CTL: during midnight to morning (from 0200–0500 to 0800–1100 LST), the coastal maritime precipitation is obviously reduced with respect to that in the WRF-CTL, in particular from 32° to 28°S, where the NDJFM-mean precipitation is reduced largely (see Figs. 4a–c and 7a–c). The precipitation around the Drakensberg almost disappears during this time period. At 1100–1400 LST, its terrestrial precipitation begins to develop in the WRF-NODB as in the WRF-CTL, but it

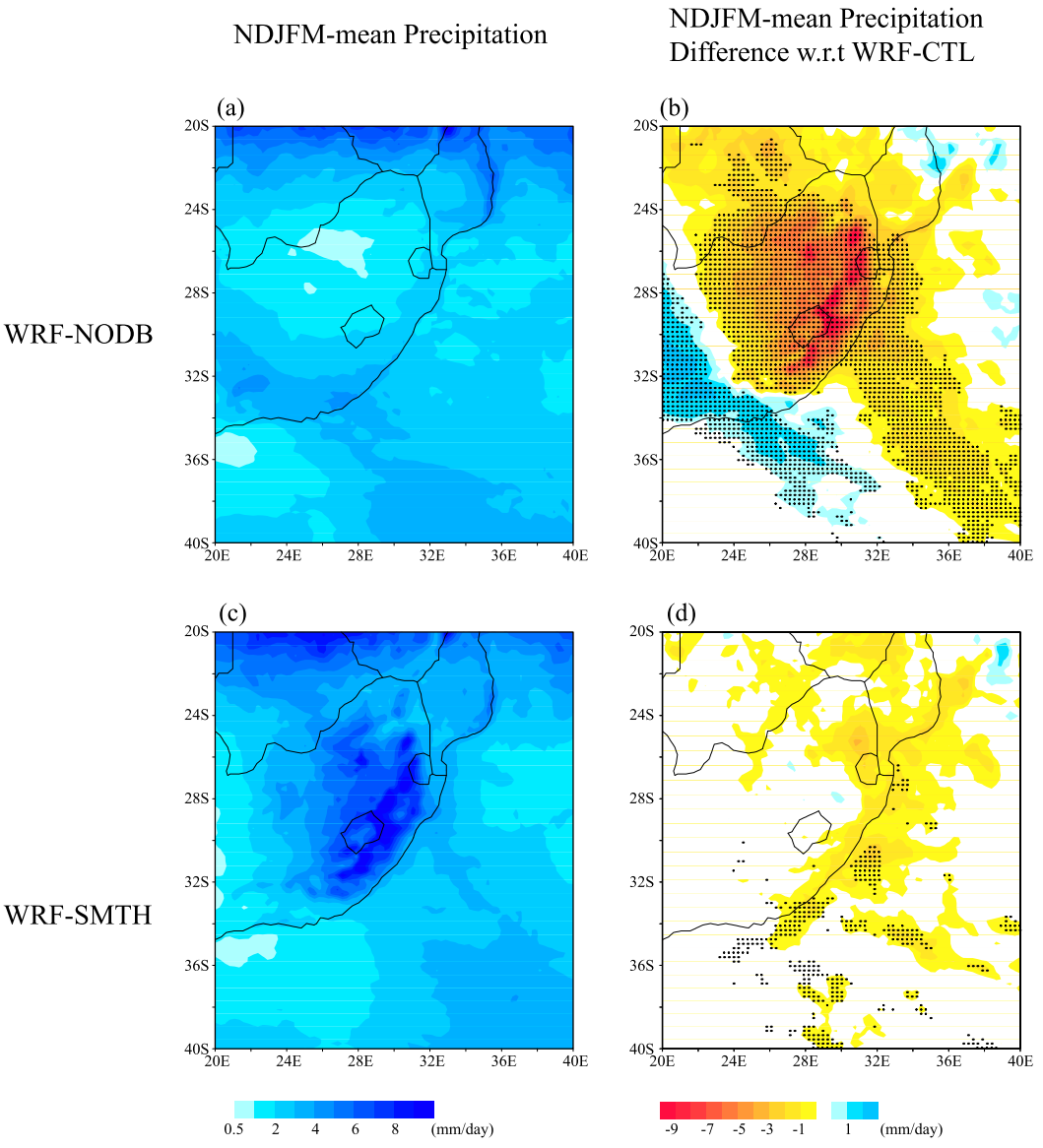

FIG. 6. From WRF-NODB simulation: (a) summer season mean precipitation distribution and (b) summer season mean precipitation difference with WRF-CTL. From WRF-SMTH simulation: (c) summer season mean precipitation distribution and (d) summer season mean precipitation difference with WRF-CTL. Black dots denote the significance level of 90%.

is concentrated only on the coastal region (Fig. 7d). At 1400–1700 LST, when the terrestrial precipitation reaches the maximum in the WRF-CTL, the precipitation produced by the WRF-NODB is also maximized over the land, but its distribution is still anchored over the coastal region. At 1700–2000 LST, the coastal precipitation is diminished. From 2000–2300 to 2300–0200 LST, the marine precipitation is generated again along the Agulhas Current (only around 34°S).

A corresponding local daily residual circulation is still detected in the WRF-NODB. In particular, the offshore land breeze is well formed at 0500–0800 LST when marine precipitation is intense. This offshore residual wind changes to onshore sea-breeze regime at 1100–1400 LST, associated with terrestrial precipitation. While at 1400–1700 LST, the onshore breeze front shifts more inward, the strong uphill valley breeze (which is seen in the WRF-CTL in Fig. 4) almost vanishes inland because of the absence of the Drakensberg highland. As a consequence, the terrestrial precipitation concentrates only along the coastal region. During midnight to early morning, the offshore land-breeze daily residual circulations are weak (Fig. 7h), in agreement with the unclear propagation of the precipitation cluster (Figs. 7g,h).

TABLE 2. Statistical value of pattern correlation between WRF-CTL and sensitivity experiments. The domain covers 40°–20°S and 20°–40°E.

	RMSE	Pattern correlation
Terrestrial precipitation (NODB)	2.9767 (mm day^{-1})	0.2314
Marine precipitation (NODB)	0.8788 (mm day^{-1})	0.6255
Terrestrial precipitation (SMTH)	0.6869 (mm day^{-1})	0.9778
Marine precipitation (SMTH)	0.5254 (mm day^{-1})	0.9167

The difference in the properties of local residual winds along the coastal region is more quantitatively systemized in Fig. 8a. The area-averaged 10-m residual wind speed at each local time $U(t)$ is calculated as

$$U(t) = \sqrt{u_s'(t)^2 + v_s'(t)^2}, \tag{3}$$

where $u_s'(t) = \frac{1}{S}\sum u'(t)$, and $v_s'(t) = \frac{1}{S}\sum v'(t)$; (4)

S is a total number of grid cells as shown in Fig. 8c. Since the grid spacing of WRF is 25 km everywhere, the contribution of area at each grid cell is equal. The quantities with a prime are the daily residual component defined by Eq. (1) at each grid point. Similarly, the area-averaged deflection angle of the 10-m daily residual winds $\Phi(t)$ is estimated by

$$\Phi(t) = \arctan\left[\frac{v_s'(t)}{u_s'(t)}\right] \quad \text{and} \quad 0 < \Phi(t) < 2\pi. \tag{5}$$

In the WRF-CTL (filled circle), the strong daily residual offshore surface flow (up to 1.5–2.0 m s^{-1}) dominates from 2300–0200 to 0500–0800 LST with an angle of $5\pi/3$ rad. The marine precipitation over the Agulhas Current is enhanced at these time periods, as shown in Fig. 4. During morning (0500–0800 LST) to early afternoon (0800–1100 LST), the daily residual

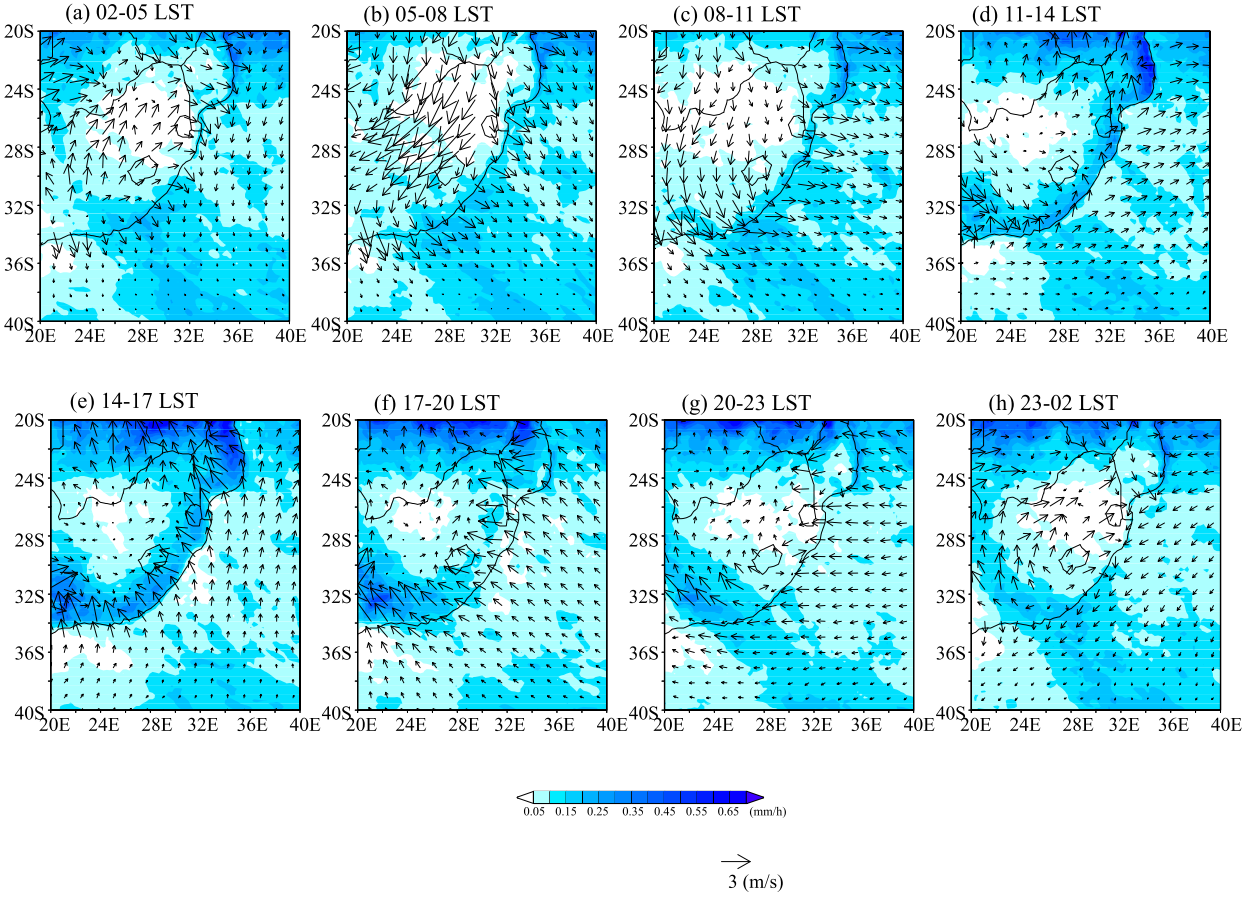

FIG. 7. As in Figs. 4a–h, but for WRF-NODB simulation.

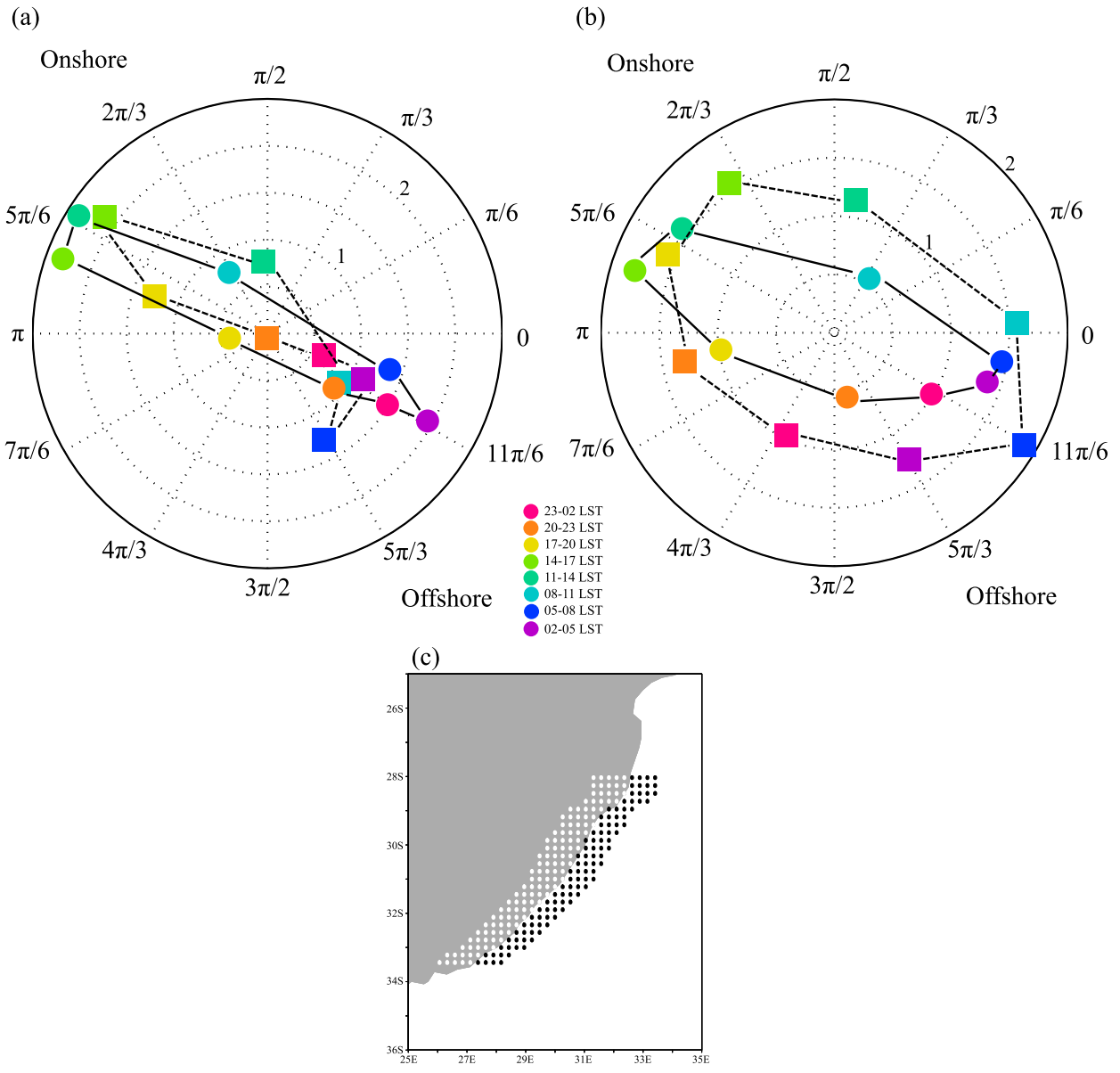

FIG. 8. (a) Three-hourly plot of area-averaged daily residual component of 10-m wind scalar (radius) and its direction from 0 to 2π in WRF-CTL (filled circle) and WRF-NODB (filled square) over the coastal land grid. Each time step is connected sequentially by solid and dashed lines in WRF-CTL and WRF-NODB. (b) As in (a), but for over the coastal ocean grid. (c) The map for the area average. The area average is performed over the white- and black-dotted grids for (a) and (b), respectively.

wind turns to an onshore breeze, changing its direction drastically to an angle of $5\pi/6$ rad. The onshore breeze is maximized at 1100–1400 to 1400–1700 LST when the terrestrial precipitation also reaches the peak (see Fig. 4). At 1700–2000 LST, the onshore flow is weakened and shifts to the offshore flow at 2000–2300 LST, again resulting in the propagation of the precipitation cluster from the land to the ocean. Because the grid points selected for this analysis contain a part of the Drakensberg, the onshore (offshore) flow can be a mixture of sea- and valley- (land and mountain) breeze circulations.

On the other hand, in the WRF-NODB (filled squares), the midnight-to-morning residual local flow is relatively weak (up to 1.2 m s^{-1}) at 2300–0200 to 0200–0500 LST. This weaker offshore breeze appears to be linked to less marine precipitation along the Agulhas Current in the WRF-NODB, compared to WRF-CTL (Figs. 7a,b). At 0500–0800 LST, the land breeze in the WRF-NODB becomes almost identical to that in the

WRF-CTL in terms of its intensity, but the meridional component is stronger in the WRF-NODB. At 0800–1100 LST, the daily residual offshore land breeze is still predominant ($1.0\,m\,s^{-1}$), while the residual surface wind switches completely to the onshore flow in the WRF-CTL. The shift in the direction of residual wind occurs at 1100–1400 LST in the WRF-NODB, while the zonal component is almost zero. But, interestingly, the offshore breeze in the WRF-NODB is amplified to more than $2.0\,m\,s^{-1}$ at 1400–1700 LST and is almost equal to that in the WRF-CTL. During evening to nighttime (1700–2000 to 2000–2300 LST), the daily residual onshore breeze is gradually weakened in the WRF-NODB, but there is no clear regime transition from the onshore to offshore breezes during midnight to early morning, as found in the WRF-CTL.

Over the Agulhas Current, in WRF-CTL, the diurnal variations in the local winds are almost identical to those over the coastal region, as shown in Fig. 8b. There is a clear change in the regime between onshore and offshore breezes while its intensity is relatively weak (up to $1.7\,m\,s^{-1}$ at 1400–1700 LST). On the other hand, in WRF-NODB, although the shift from onshore to offshore breeze can be still seen, the meridional component is largely dominant, compared to that in WRF-CTL. Another modification is that there is a delay of the diurnal variation in local winds in WRF-NODB. For instance, while the strongest onshore wind is at 1400–1700 LST in WRF-CTL, it occurs at 1700–2000 LST in WRF-NODB. A similar delay is detected in the regime of offshore breeze as well (at 0200–0800 LST in WRF-CTL and at 0500–1100 LST in WRF-SMTH in Figs. 8a,b).

c. *Diurnal cycle in the WRF-SMTH*

Figure 9 gives the difference in 3-hourly precipitation between the WRF-SMTH and WRF-CTL. From 0200–0500 to 0800–1100 LST, the significant reduction in precipitation is detected over the coastal sea along the Agulhas Current. On the other hand, the terrestrial precipitation over the coastal region is more effectively reduced from 1100–1400 to 1700–2000 LST (afternoon to evening), but its significance is quite weak. Again, the marine rainfall is more diminished from 2000–2300 to 2300–0200 LST with some significance. This cycle seems to be consistent with the cycle of sea- and land-breeze circulation. As shown in Fig. 10a, the WRF-SMTH simulates quite an identical diurnal variation in residual surface winds to that in the WRF-CTL. This suggests that the warm SST associated with the Agulhas Current is not a main driver of the daily varying local circulation.

The difference in the latent heat flux is presented in Fig. 10b. Since in the WRF-SMTH, the smoothing cools the warm SST associated with the Agulhas Current, the atmospheric gain of the water vapor is reduced in the WRF-SMTH. At largest, 30% of the latent heat flux is reduced in the WRF-SMTH along the Agulhas Current. Nkwinkwa Njouodo et al. (2018) showed that the low-level convergence and associated coastal marine precipitation are enhanced by the warm SST due to the Agulhas Current with the same results of WRF simulations. During the night and morning (0200–0500 to 0800–1100 LST), the low-level convergence is weakened along the Agulhas Current (not shown). This convergence is associated with the collision of offshore land breeze and onshore background wind. This alleviation of the convergence is attributed to less marine precipitation during the night and morning (Fig. 9). On the other hand, during the daytime, the weakened low-level convergence along the Agulhas Current may not affect the onshore sea-breeze front over the land and terrain.

d. *Sensitivity to choices of model version and physical scheme*

The previous subsection showed that the Drakensberg is a major player for forming precipitation and its diurnal variation, while the sharp SST gradient of the Agulhas Current has a secondary importance for the region. As previous studies demonstrated (Pohl et al. 2014; Mooney et al. 2017), the simulation of precipitation (over South Africa and the United States) is dependent on the cumulus convection scheme. Thus, altering the latter could modify our conclusions based on a unique physical package. Therefore, in this section, we perform sensitivity experiments to address the scheme dependency of our results. In addition, as the WRF system is an open source, frequently updated model, we explore the version dependency as well.

Additional experiments are performed with version 3.9.1 of WRF and three different cumulus convection schemes: Kain–Fritsch (KF; Kain 2004), Betts–Miller–Janjić (BMJ; Janjić 1994), and Grell–Freitas (GF; Grell and Freitas 2014). All other settings in the model and experimental setup are identical to those in WRF-CTL [see section 2b(1)]. Two experiments, one with and one without the Drakensberg, are performed with each convective scheme. Each experiment is integrated from 1 December 2000 to 1 April 2002, and we analyze the results of November–March in 2001/02 (after a 1-yr-long spinup period). Because the sharp SST gradient associated with the Agulhas Current plays a relatively minor role for the precipitation (see sections 4b and 4c), we do not further address its role in this section.

Results are summarized in Table 3. We use the data of NDJFM in 2001/02 for WRF version 3.7.1 with KF from WRF-CTL (hereafter, KF-3.7.1). Between the two versions of WRF with KF, the simulated rainfall

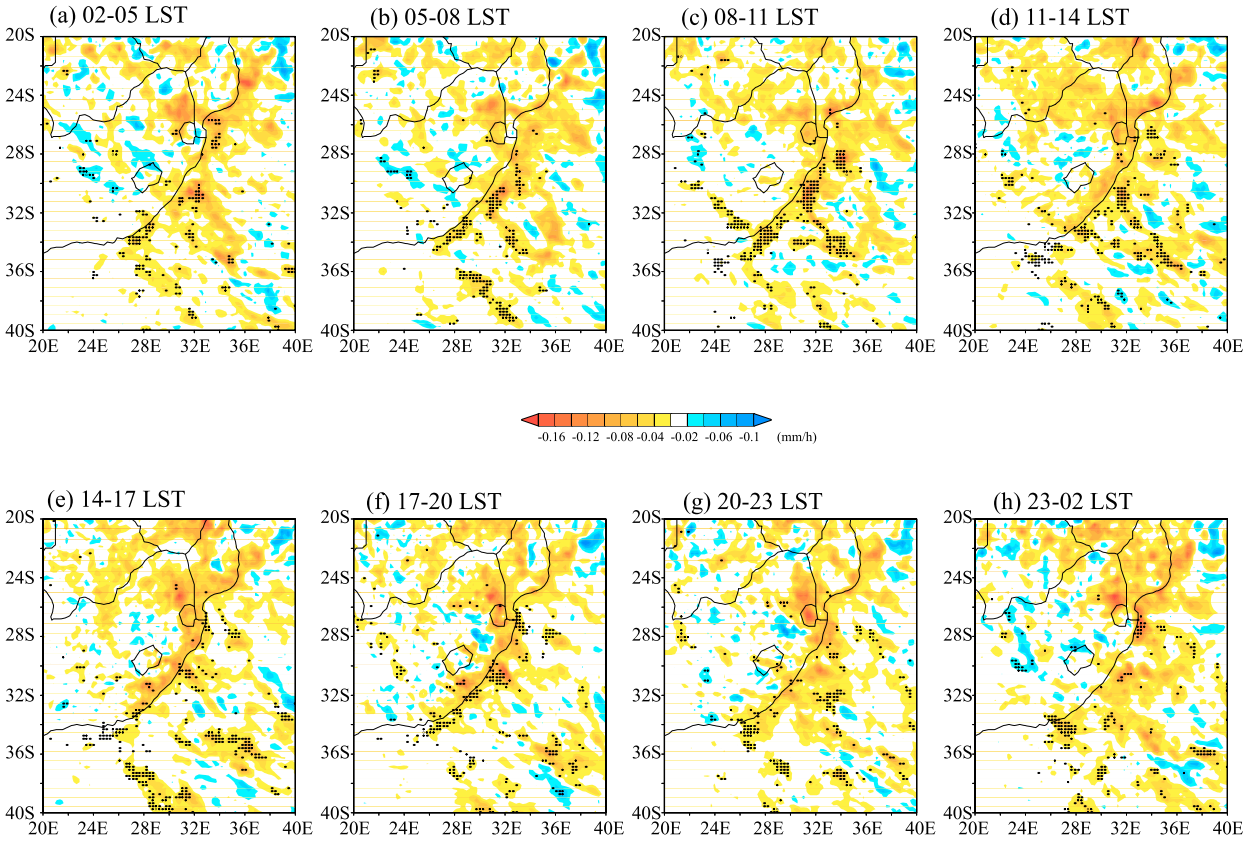

FIG. 9. As in Figs. 4a–h, but for the difference between WRF-SMTH and WRF-CTL simulations only for precipitation. Black dots denote the significance level of 90%.

and its response to the Drakensberg is approximately equal around the Drakensberg and over the Agulhas Current, implying that the effects of topography are not sensitive to the model version as long as the cumulus scheme is identical (there are some improvements of other physical schemes; for details, see https://www.mmm.ucar.edu/wrf-release-information). In contrast, the response of rainfall to the flattened land surface shows some scheme dependency. The terrestrial rainfall around the Drakensberg is reduced significantly in BMJ and GF, although its reduction rate is slightly less than that in KF (−69.35/−67.74, −64.85, and −63.98% for KF-3.7.1/KF, BMJ, and GF, respectively). This result suggests our assessment of the Drakensberg impact on the land precipitation is robust. Interestingly, marine rainfall over the Agulhas Current is less sensitive to the presence of the Drakensberg in BMJ and GF (−42.28/−46.23, −36.30, and −29.55% for KF-3.7.1/KF, BMJ, and GF, respectively). It can be argued that the choice of cumulus convection needs to be paid more attention for the simulation of marine precipitation. On the other hand, the horizontal pattern of precipitation response to no topography in each experiment is approximately similar to that of Fig. 6b (not shown), thereby suggesting that the first-order influence of the Drakensberg is independent of the cumulus scheme.

Since Pohl et al. (2014) have already done a detailed investigation on physics dependency of the rainfall and its diurnal cycle, this study does not investigate the sensitivity of diurnal cycle with different cumulus schemes. On the other hand, correspondingly to the results of Table 3, the daytime (evening–nighttime) precipitation around the Drakensberg (over the Agulhas Current) is reduced similarly in each sensitivity experiment (not shown). This assessment can make the results of the comparison between WRF-CTL and WRF-NODB more robust.

5. Summary and discussion

In this study, the summertime diurnal variations in precipitation and local circulation over eastern South Africa are investigated using observed datasets and WRF Model simulations. In particular, we explore the possible roles of the two components of the lower-boundary conditions for the diurnal cycle: a complex topography of the Drakensberg and a sharp warm SST front due to the Agulhas Current. Figure 11 summarizes

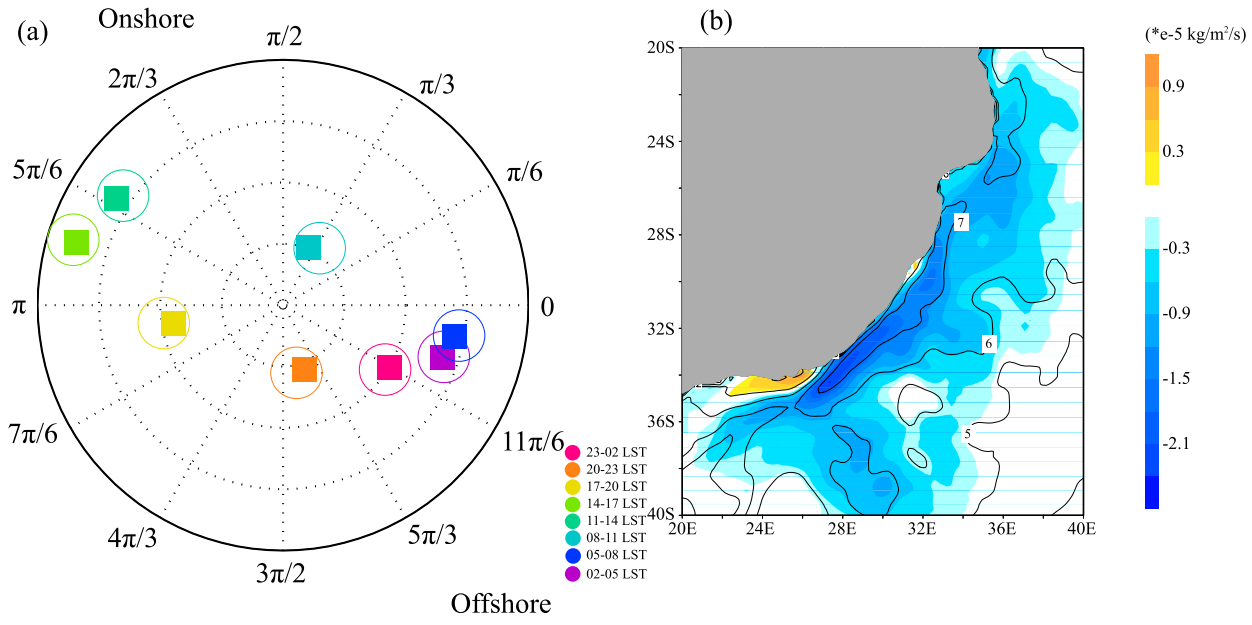

FIG. 10. (a) As in Fig. 8b, but for WRF-CTL (open circle) and WRF-SMTH (filled square). (b) NDJFM-mean evaporation difference between WRF-SMTH and WRF-CTL (color) superimposing NDJFM-mean evaporation in WRF-CTL (contour; CI; 1×10^{-4} kg m^2 s^{-1}).

the results of a series of numerical simulations throughout this study.

a. *Capability of the WRF to reproduce the climate*

The WRF's benchmark simulation (WRF-CTL) is able to represent the observed hydrometeorological climates in the region reasonably well, although terrestrial precipitation is overestimated, particularly around the Drakensberg (Figs. 11b,c). While the diurnal variations in precipitation and daily residual breeze systems are also reasonably reproduced, the timing of maximum terrestrial precipitation is simulated slightly earlier (1400–1700 LST) than in the observations (1700–2000 LST; Figs. 11b,c). This is a common problem for precipitation in regional climate modeling (e.g., Nikulin et al. 2012; Pohl et al. 2014). On the other hand, the marine precipitation over the Agulhas Current (Fig. 11d) is better reproduced in terms of amount in spite of slightly delayed timing of precipitation maximum (2300–0200 LST in WRF-CTL and 2000–2300 LST in observation). These variations in precipitations are associated with the daily residual local circulations: when the terrestrial (marine) precipitation is dominant, the onshore and uphill (offshore and downhill) breeze systems are formed around the Drakensberg and coastal South Africa. Although the amplitude of diurnal variation is quite small over the open ocean (Fig. 5), the SICZ precipitation is slightly large during midnight to morning. WRF-CTL represents the SICZ quite well (Fig. 11e).

b. *Roles of lower-boundary conditions for diurnal variations*

The sensitivity experiments with WRF have elucidated that the Drakensberg is important, but the SST is

TABLE 3. NDJFM-mean rainfall in 2001/02 averaged around the Drakensberg and over the Agulhas Current for each sensitivity experiment of model and physics choice. Averaging area of the Drakensberg and Agulhas Current is given in Fig. 11a.

	Kain–Fritsch (v3.7.1)	Kain–Fritsch (v3.9.1)	Betts–Miller–Janjić	Grell–Freitas
(a) Rainfall (mm day^{-1}) around the Drakensberg	7.515	7.368	5.592	6.974
(b) Rainfall (mm day^{-1}) around the Drakensberg (no topography)	2.303	2.377	1.966	2.512
(c) $100 \times$ [(b)−(a)]/(a)(%)	−69.35	−67.74	−64.85	−63.98
(d) Rainfall (mm day^{-1}) over the Agulhas	3.817	3.807	2.788	4.322
(e) Rainfall (mm day^{-1}) over the Agulhas (no topography)	2.203	2.047	1.776	3.045
(f) $100 \times$ [(e)−(d)]/(d)(%)	−42.28	−46.23	−36.30	−29.55

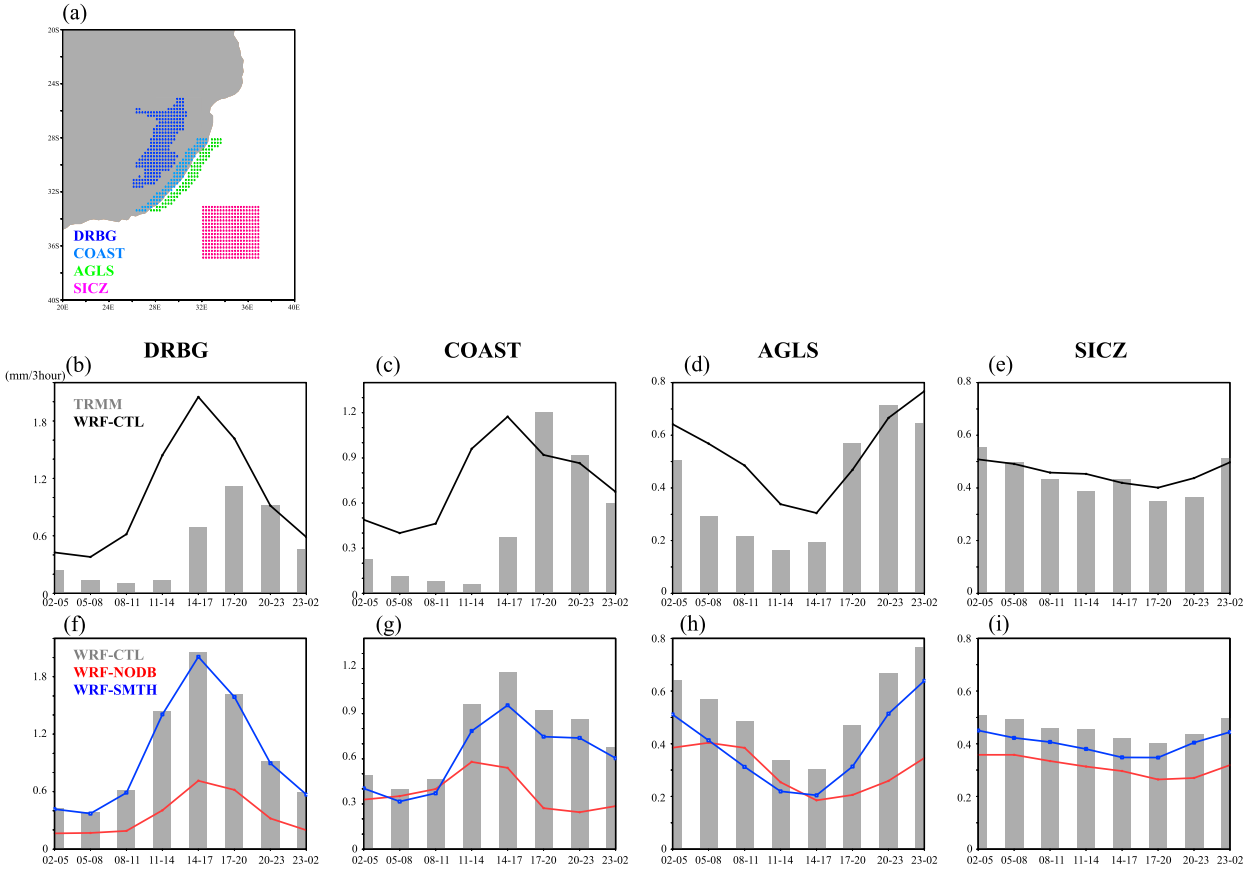

FIG. 11. (a) Selected grid for averaging 3-hourly rainfall at the Drakensberg (DRBG; blue), coastal region (COAST; light blue), Agulhas Current (AGLS; green), and SICZ (magenta). For DRBG, the grids where the topography height is higher than 1500 m are selected. (b)–(e) Area-averaged 3-hourly rainfall in TRMM (gray bar) and WRF-CTL (black line) and (f)–(i) in WRF-CTL (gray bar), WRF-NODB (red line), and WRF-SMTH (blue line).

not for the diurnal variations in this region. Most outstandingly, the terrestrial precipitation is reduced in WRF-NODB, and its amplitude of diurnal variation is largely weakened (Figs. 11f,g). In the absence of the Drakensberg, the daily residual onshore and uphill local breeze is also weakened, and, consequently, the terrestrial precipitation is diminished. In particular, because the daily residual breeze is well associated with the topographic gradient of the Drakensberg (Fig. 5), the uphill valley breeze is not driven without the Drakensberg, although the sea-breeze circulation is still alive with some modulations in direction and intensity (Figs. 7 and 8). Furthermore, since there is no orographic uplifting effect around the Drakensberg in WRF-NODB, the daytime precipitation over the land is largely diminished. Interestingly, the marine precipitation and its diurnal variation are also damped in WRF-NODB (Fig. 11h). The nocturnal precipitation is reduced to about 50% of that in WRF-CTL, while the daytime precipitation is reduced modestly. This result can be linked to the weakened offshore and downhill breeze systems during midnight to morning (Figs. 7 and 8). Because the daily mean background wind is generally easterly associated with the Mascarene high pressure (Fig. 2d), the offshore breeze collides with the easterly, and, consequently, the convergence is enhanced along the coast. Without the Drakensberg, the background wind is more easterly due to the cyclonic anomaly (see Fig. S1 in the online supplemental material). However, the daily residual wind during midnight to early morning is quite weak, and its direction is easterly (2300–0200 and 0200–0500 LST) and almost southward (0500–0800 LST) when the westerly offshore land breezes are predominant in WRF-CTL (Figs. 4, 7, 8a,b). Under such conditions, the convergence may not be formed effectively. Therefore, the coastal precipitation is suppressed, especially during these periods (Fig. 11h). In addition, the absence of the Drakensberg forces the larger-scale high SLP and lower-tropospheric geopotential height anomaly over eastern South Africa to the south Indian Ocean (see Fig. S2 in the

supplemental material). This anomaly can also inhibit cumulus convection and associated precipitation over the ocean. In particular, the precipitation in the SICZ is reduced, as shown in Fig. 11i.

On the other hand, the warm SST due to the Agulhas Current does not affect the inland precipitation and its diurnal variation around the Drakensberg (Fig. 11f). This is because the onshore and uphill breezes are not influenced by the warm SST along the eastern coast of South Africa (Figs. 9 and 10a). Conversely, the coastal precipitation over the land and ocean is reduced, and its amount of reduction is roughly identical throughout a day (Figs. 11g,h). While the narrow band of warm SST due to the Agulhas Current is not of importance for regulating the local diurnal cycle, the warm SST supplies the water vapor effectively (e.g., Nkwinkwa Njouodo et al. 2018; Fig. 10b) and helps the precipitation to be enhanced along the coastal region (e.g., Jury et al. 1993; Rouault et al. 2013; Nkwinkwa Njouodo et al. 2018). These lower-boundary conditions influence not only surface precipitation, but also the troposphere (not shown). Corresponding to larger changes in the precipitation, WRF-NODB shows the larger anomaly in the tropospheric geopotential height than in WRF-SMTH. Especially, the Drakensberg plays a role for large-scale atmospheric circulation (e.g., Potter et al. 2017). The impacts of the Drakensberg on the continental-scale climate are investigated in our other study (Koseki and Demissie 2018).

This study has revealed that the Drakensberg plays a crucial role for local weather systems, and, additionally, synoptic-scale atmospheric circulation is modified by the Drakensberg over the south Indian Ocean. For further investigations, there is a need to understand more deeply how the Drakensberg influences the subtropical climate over the south Indian Ocean in terms of formation of low-level stratocumulus and the intertropical convergence zone, as Richter and Mechoso (2004) and Potter et al. (2017) have done research over the southern Atlantic Ocean. On the other hand, while the response of the terrestrial rainfall to the topography is rather robust with respect to the three different convection schemes tested here, the response of the marine rainfall over the Agulhas Current is more scheme dependent.

Acknowledgments. We greatly appreciate one anonymous reviewer and Prof. Richard Washington at Keble College, Oxford, for their constructive reviewing comments. And we thank to Dr. Ricardo Fonseca at Luelå University of Technology and Dr. Susana Mendes Reuder at University of Bergen for their technical help in conducting the numerical experiments and analyzing the outputs of WRF. Also, we would like to express our thanks to Prof. Dr. Mathieu Rouault at the University of Cape Town and Dr. Priscilla A. Mooney at NORCE for the discussion for initiating this work and helpful discussions on the diurnal cycle. S. Koseki received financial support from the EU FP7/2007-2013 PREFACE project (Grant Agreement 603521), ERC STERCP project (Grant Agreement 64982), NFR-PREFACE (233680/E10), and NFR-SCAMPI project.

REFERENCES

Backeberg, B. C., L. Bertino, and J. A. Johannessen, 2009: Evaluating two numerical advection schemes in HYCOM for eddy-resolving modelling of the Agulhas Current. *Ocean Sci.*, **5**, 173–190, https://doi.org/10.5194/os-5-173-2009.

Bhatt, B. C., S. Sobolowski, and A. Higuchi, 2016: Simulation of diurnal rainfall variability over the Maritime Continent with a high-resolution regional climate model. *J. Meteor. Soc. Japan*, **94A**, 89–103, https://doi.org/10.2151/jmsj.2015-052.

Boebel, O., J. Lutjeharms, C. Schmid, W. Zenk, T. Rossby, and C. Barron, 2003: The Cape cauldron: A regime of turbulent inter-ocean exchange. *Deep-Sea Res. II*, **50**, 57–86, https://doi.org/10.1016/S0967-0645(02)00379-X.

Chen, F., and J. Dudhia, 2001a: Coupling an advanced land surface–hydrology model with the Penn State–NCAR MM5 modeling system. Part I: Model implementation and sensitivity. *Mon. Wea. Rev.*, **129**, 569–585, https://doi.org/10.1175/1520-0493(2001)129<0569:CAALSH>2.0.CO;2.

——, and ——, 2001b: Coupling an advanced land surface–hydrology model with the Penn State–NCAR MM5 modeling system. Part II: Preliminary model validation. *Mon. Wea. Rev.*, **129**, 587–604, https://doi.org/10.1175/1520-0493(2001)129<0587:CAALSH>2.0.CO;2.

——, and Coauthors, 2007: Description and evaluation of the characteristics of the NCAR high-resolution land data assimilation system. *J. Appl. Meteor. Climatol.*, **46**, 694–713, https://doi.org/10.1175/JAM2463.1.

Chen, S. S., and R. A. Houze, 1997: Diurnal variation and life-cycle of deep convective systems over the tropical Pacific warm pool. *Quart. J. Roy. Meteor. Soc.*, **123**, 357–388, https://doi.org/10.1002/qj.49712353806.

Cook, K. H., 2000: The South Indian convergence zone and interannual rainfall variability over southern Africa. *J. Climate*, **13**, 3789–3804, https://doi.org/10.1175/1520-0442(2000)013<3789:TSICZA>2.0.CO;2.

Cosgrove, B. A., and Coauthors, 2003: Land surface model spin-up behavior in the North American Land Data Assimilation System (NLDAS). *J. Geophys. Res.*, **108**, 8845, https://doi.org/10.1029/2002JD003316.

Crétat, J., C. Macron, B. Pohl, and Y. Richard, 2011: Quantifying internal variability in a regional climate model: A case study for southern Africa. *Climate Dyn.*, **37**, 1335–1356, https://doi.org/10.1007/s00382-011-1021-5.

Dee, D. P., and Coauthors, 2011: The ERA-Interim reanalysis: Configuration and performance of the data assimilation system. *Quart. J. Roy. Meteor. Soc.*, **137**, 553–597, https://doi.org/10.1002/qj.828.

Estoque, M. A., 1962: The sea breeze as a function of the prevailing synoptic situation. *J. Atmos. Sci.*, **19**, 244–250, https://doi.org/10.1175/1520-0469(1962)019<0244:TSBAAF>2.0.CO;2.

Gergis, J., and B. J. Henley, 2017: Southern Hemisphere rainfall variability over the past 200 years. *Climate Dyn.*, **48**, 2087–2105, https://doi.org/10.1007/s00382-016-3191-7.

Grell, G. A., and S. R. Freitas, 2014: A scale and aerosol aware stochastic convective parameterization for weather and air quality modeling. *Atmos. Chem. Phys.*, **14**, 5233–5250, https://doi.org/10.5194/acp-14-5233-2014.

Hong, S. Y., and J.-O. J. Lim, 2006: The WRF Single-Moment 6-Class Microphysics scheme (WSM6). *J. Kor. Meteor. Soc.*, **42**, 129–151.

——, Y. Noh, and J. Dudhia, 2006: A new vertical diffusion package with an explicit treatment of entrainment processes. *Mon. Wea. Rev.*, **134**, 2318–2341, https://doi.org/10.1175/MWR3199.1.

Huffman, G. J., and Coauthors, 2007: The TRMM Multisatellite Precipitation Analysis (TMPA): Quasi-global, multiyear, combined-sensor precipitation estimates at fine scales. *J. Hydrometeor.*, **8**, 38–55, https://doi.org/10.1175/JHM560.1.

Janjić, Z., 1994: The step-mountain eta coordinate model: Further developments of the convection, viscous sublayer, and turbulence closure schemes. *Mon. Wea. Rev.*, **122**, 927–945, https://doi.org/10.1175/1520-0493(1994)122<0927:TSMECM>2.0.CO;2.

Joseph, B., B. C. Bhatt, T.-Y. Koh, and S. Chen, 2008: Sea breeze simulation over the Malay Peninsula in an intermonsoon period. *J. Geophys. Res.*, **113**, D20122, https://doi.org/10.1029/2008JD010319.

Jury, M. R., H. R. Valentine, and J. R. Lutjeharms, 1993: Influence of the Agulhas Current on summer rainfall along the southeast coast of South Africa. *J. Appl. Meteor.*, **32**, 1282–1287, https://doi.org/10.1175/1520-0450(1993)032<1282:IOTACO>2.0.CO;2.

Kain, J. S., 2004: The Kain–Fritsch convective parameterization: An update. *J. Appl. Meteor.*, **43**, 170–181, https://doi.org/10.1175/1520-0450(2004)043<0170:TKCPAU>2.0.CO;2.

Koseki, S., and T. Demissie, 2018: Does the Drakensberg dehydrate southwestern Africa? *J. Arid Environ.*, **158**, 35–42, https://doi.org/10.1016/j.jaridenv.2018.08.003.

——, T.-Y. Koh, and C.-K. Teo, 2013: Effects of the cold tongue in the South China Sea on the monsoon, diurnal cycle and rainfall in the Maritime Continent. *Quart. J. Roy. Meteor. Soc.*, **139**, 1566–1582, https://doi.org/10.1002/qj.2052.

Lawal, K. A., D. A. Stone, T. Aina, C. Rye, and B. J. Abiodun, 2015: Trends in the potential spread of seasonal and climate simulations over South Africa. *Int. J. Climatol.*, **35**, 2193–2209, https://doi.org/10.1002/joc.4234.

Li, L., I. Diallo, C. Y. Xu, and F. Stordal, 2015: Hydrological projections under climate change in the near future by RegCM4 in southern Africa using a large-scale hydrological model. *J. Hydrol.*, **528**, 1–16, https://doi.org/10.1016/j.jhydrol.2015.05.028.

Lutjeharms, J. R. E., R. D. Mey, and I. T. Hunter, 1986: Cloud lines over the Agulhas Current. *S. Afr. J. Sci.*, **82**, 635–640.

MacKella, N., M. New, and C. Jack, 2014: Observed and modelled trends in rainfall and temperature for South Africa: 1960–2010. *S. Afr. J. Sci.*, **110**, 1–13, https://doi.org/10.1590/sajs.2014/20130353.

McNally, A., and Coauthors, 2017: A land data assimilation system for sub-Saharn Africa flood and water security applications. *Sci. Data*, **4**, 170012, https://doi.org/10.1038/sdata.2017.12.

Mlawer, E., S. Taubman, P. Brown, M. Iacono, and S. Clough, 1997: Radiative transfer for inhomogeneous atmosphere: RRTM, a validated correlated-k model for the longwave. *J. Geophys. Res.*, **102**, 16 663–16 682, https://doi.org/10.1029/97JD00237.

Mooney, P. A., C. Broderick, C. L. Bruyère, F. J. Mulligan, and A. F. Prein, 2017: Clustering of observed diurnal cycles of precipitation over the United States for evaluation of a WRF multiphysics regional climate ensemble. *J. Climate*, **30**, 9267–9286, https://doi.org/10.1175/JCLI-D-16-0851.1.

Nesbitt, S. W., and E. J. Zipser, 2003: The diurnal cycle of rainfall and convective intensity according to three years of TRMM measurements. *J. Climate*, **16**, 1456–1475, https://doi.org/10.1175/1520-0442-16.10.1456.

Nikulin, G., and Coauthors, 2012: Precipitation climatology in an ensemble of CORDEX-Africa regional climate simulations. *J. Climate*, **25**, 6057–6078, https://doi.org/10.1175/JCLI-D-11-00375.1.

Nkwinkwa Njouodo, A. S., S. Koseki, N. Keenlyside, and M. Rouault, 2018: Atmospheric signature of the Agulhas Current. *Geophys. Res. Lett.*, **45**, 5185–5193, https://doi.org/10.1029/2018GL077042.

Pohl, B., Y. Richard, and N. Fauchereau, 2007: Influence of the Madden–Julian oscillation on southern African summer rainfall. *J. Climate*, **20**, 4227–4242, https://doi.org/10.1175/JCLI4231.1.

——, M. Rouault, and S. S. Roy, 2014: Simulation of the annual and diurnal cycles of rainfall over South Africa by a regional climate model. *Climate Dyn.*, **43**, 2207–2226, https://doi.org/10.1007/s00382-013-2046-8.

Potter, S. F., E. J. Dawson, and D. M. W. Frierson, 2017: Southern African orography impacts on low clouds and the Atlantic ITCZ in a coupled model. *Geophys. Res. Lett.*, **44**, 3283–3289, https://doi.org/10.1002/2017GL073098.

Preston-Whyte, R. A., 1970a: Land breezes and rainfall on the Natal Coast. *S. Afr. Geogr. J.*, **52**, 38–43, https://doi.org/10.1080/03736245.1970.10559463.

——, 1970b: Local atmospheric circulations and the mesoclimate of Durban. Ph.D. thesis, University of Natal, 237 pp., https://researchspace.ukzn.ac.za/xmlui/handle/10413/5463.

Reynolds, R. W., T. M. Smith, C. Liu, D. B. Chelton, K. S. Casey, and M. G. Schlax, 2007: Daily high-resolution-blended analyses for sea surface temperature. *J. Climate*, **20**, 5473–5496, https://doi.org/10.1175/2007JCLI1824.1.

Richter, I., and C. R. Mechoso, 2004: Orographic influences on the annual cycle of Namibian stratocumulus clouds. *Geophys. Res. Lett.*, **31**, L24108, https://doi.org/10.1029/2004GL020814.

Rouault, M., S. S. Roy, and R. C. Balling Jr., 2013: The diurnal cycle of rainfall in South Africa in the austral summer. *Int. J. Climatol.*, **33**, 770–777, https://doi.org/10.1002/joc.3451.

Skamarock, W. C., and Coauthors, 2008: A description of the Advanced Research WRF version 3. NCAR Tech. Note NCAR/TN-475+STR, 113 pp., https://doi.org/10.5065/D68S4MVH.

Teo, C.-K., T.-Y. Koh, J. C.-F. Lo, and B. C. Bhatt, 2011: Principal component analysis of observed and modeled diurnal rainfall in the Maritime Continent. *J. Climate*, **24**, 4662–4675, https://doi.org/10.1175/2011JCLI4047.1.

Tyson, P. D., 1968a: Nocturnal local winds in a Drakensberg valley. *S. Afr. Geogr. J.*, **50**, 15–32, https://doi.org/10.1080/03736245.1968.10559428.

——, 1968b: A note on the nomenclature of the topographically-induced local winds of Natal. *S. Afr. Geogr. J.*, **50**, 133–134, https://doi.org/10.1080/03736245.1968.10559429.

——, and R. A. Preston-Whyte, 1972: Observations of regional topographically-induced wind systems in Natal. *J. Appl. Meteor.*, **11**, 643–650, https://doi.org/10.1175/1520-0450(1972)011<0643:OORTIW>2.0.CO;2.

Webb, C. J., 1999: An analytic model of the Agulhas Current as a western boundary current with linearly varying viscosity. *J. Phys. Oceanogr.*, **29**, 1517–1527, https://doi.org/10.1175/1520-0485(1999)029<1517:AAMOTA>2.0.CO;2.

Yang, S., and E. A. Smith, 2006: Mechanism for diurnal variability of global tropical rainfall observed from TRMM. *J. Climate*, **19**, 5190–5226, https://doi.org/10.1175/JCLI3883.1.